Applied Physics Letters

Elucidating possible crystallographic origins of wake-up mechanisms in ferroelectric hafnia

Cite as: Appl. Phys. Lett. **118**, 092902 (2021); https://doi.org/10.1063/5.0029691
Submitted: 15 September 2020 • Accepted: 12 February 2021 • Published Online: 02 March 2021

Sean R. C. McMitchell, Sergiu Clima, Nicolo' Ronchi, et al.

COLLECTIONS

Paper published as part of the special topic on Ferroelectricity in Hafnium Oxide: Materials and Devices

ARTICLES YOU MAY BE INTERESTED IN

Next generation ferroelectric materials for semiconductor process integration and their applications
Journal of Applied Physics **129**, 100901 (2021); https://doi.org/10.1063/5.0037617

Ferroelectricity in hafnium oxide thin films
Applied Physics Letters **99**, 102903 (2011); https://doi.org/10.1063/1.3634052

Impact of area scaling on the ferroelectric properties of back-end of line compatible $Hf_{0.5}Zr_{0.5}O_2$ and Si:HfO_2-based MFM capacitors
Applied Physics Letters **118**, 062904 (2021); https://doi.org/10.1063/5.0035650

© 2021 Author(s).

Elucidating possible crystallographic origins of wake-up mechanisms in ferroelectric hafnia

Cite as: Appl. Phys. Lett. **118**, 092902 (2021); doi: 10.1063/5.0029691
Submitted: 15 September 2020 · Accepted: 12 February 2021 ·
Published Online: 2 March 2021

View Online

Export Citation

CrossMark

Sean R. C. McMitchell,[1,a)] Sergiu Clima,[1] Nicolo' Ronchi,[1] Kaustuv Banerjee,[1] Umberto Celano,[1,2] Mihaela Popovici,[1] Luca Di Piazza,[1] Geert Van den Bosch,[1] and Jan Van Houdt[1,3]

AFFILIATIONS

[1]imec, Kapeldreef 75, B-3001 Heverlee (Leuven), Belgium
[2]Faculty of Science and Technology and MESA+ Institute for Nanotechnology, University of Twente, 7522 NH Enschede, The Netherlands
[3]Physics and Astronomy, KU Leuven, 3000 Leuven, Belgium

Note: This paper is part of the Special Topic on Materials and Devices Utilizing Ferroelectricity in Halfnium Oxide.
[a)]**Author to whom correspondence should be addressed:** sean.mcmitchell@imec.be

ABSTRACT

The wake-up in doped hafnia ferroelectric devices is an extremely important process to understand in order to integrate these materials successfully into working ferroelectric memory devices. The crystallographic origins of this process are clarified with three main mechanisms. Strain relaxation in the ferroelectric orthorhombic phase led to an adjustment of the unit cell volume toward a "bulk-like" value. The undistorted cell allowed for easier polarizability within the unit cell, allowing higher polarization. Reversible phase transformations between the tetragonal and orthorhombic phases depend on the nature of the strain. Finally, a model is developed describing grain reorientation, inducing a 90° rotation of the orthorhombic unit cell and allowing the phase to respond to the E-field more readily under cycling.

Published under license by AIP Publishing. https://doi.org/10.1063/5.0029691

Recently, there has been much interest around ferroelectric doped hafnia due to it being scalable to sub-10 nm thicknesses, lead-free, and CMOS compatible. These properties along with the nonvolatile nature of ferroelectric materials yield promise for integration in current technology nodes for low-power, high-density memory.[1] Both academia and industry have shown interest in this material, demonstrating both ferroelectric field effect transistors (FeFETs) and capacitors (Fe-RAM) with both vertical and planar device geometries.[2–6] Hafnia is common in CMOS technologies and so is fab compatible. However, it is an inherently multiphasic material with centrosymmetric phases (monoclinic, tetragonal, and cubic) being native to the material. With the introduction of strain imposed by dopants (intrinsic),[7–9] interfacial materials (extrinsic),[10] or thermal anneals, a noncentrosymmetric orthorhombic phase can be generated that is ferroelectric.[1,11,12] This multiphasic nature adds complexity to the ferroelectric response due to the ferroelectric phase domains being embedded in a paraelectric matrix.[13] As such, there are several possible crystallographic mechanisms to explain the typical wake-up, that is, the process in conditioning the ferroelectric layer to yield optimum polarization hysteresis [Fig. 1(b)]. In metal–ferroelectric–metal (MFM) capacitors, the wake-up occurs over many E-field cycles with the ferroelectric hysteresis loop opening from an antiferroelectric-like pinched loop to a fully open hysteretic behavior. In silicon–ferroelectric–silicon (SFS) capacitors, the wake-up is often shorter, starting with an open hysteretic behavior, but the remnant polarization (P_r) increases with cycling. Here, identification of possible wake-up mechanisms is attempted through probing cycled device structures by grazing incidence X-ray diffraction (GIXRD), while using density functional theory (DFT) calculations as a guide in analysis.

Amorphous doped hafnia layers were grown with a thickness of 8–10 nm using atomic layer deposition (ALD) on 300 mm Si (100) wafers. A process temperature of 300 °C was used with $HfCl_4$ and H_2O precursors. Dopant [Al (7% doping) or Si (3.6% doping)] oxide layers were inserted by adjusting the pulse ratio of Hf and dopant layers in deposition. In SFS stacks, doped hafnia was deposited directly onto a Si wafer (~1 nm SiO_2 interface) before being capped with 50 nm amorphous Si. No evidence of Si diffusion between the Si-doped hafnia layer and electrode material was found. In MFM stacks, the hafnia layer was deposited on a 10 nm TiN bottom electrode, before 10 nm TiN was deposited as a top electrode. The deposition is followed by a crystallization anneal between 620 and 1000 °C depending on the dopant and electrode type. The top electrode layer of each wafer was etched in a fab-based photolithographic process

Published under license by AIP Publishing

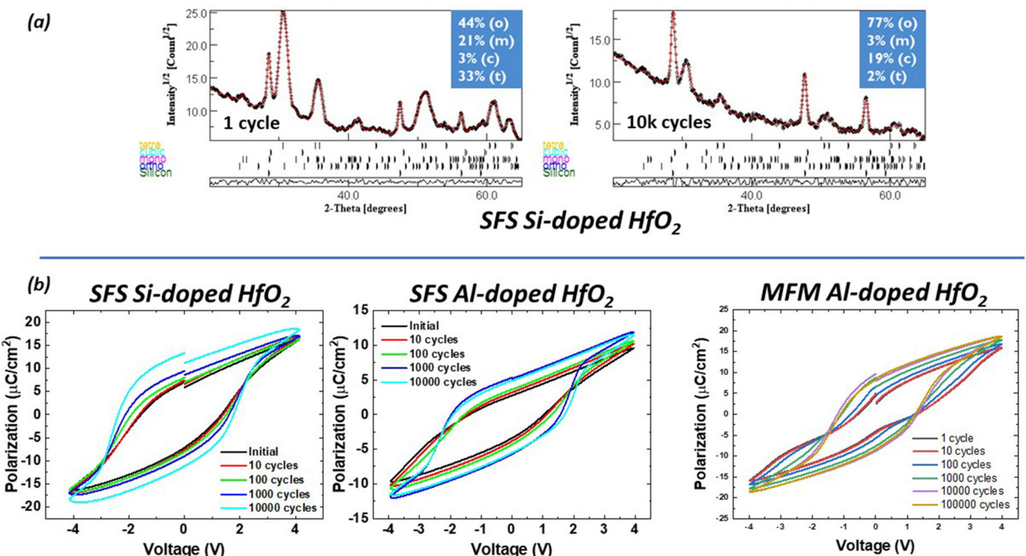

FIG. 1. Phase composition evolution with E-field cycling of an SFS stack with 8 nm Si-doped hafnia (a) and ferroelectric hysteresis loops for Si- and Al-doped hafnia in both SFS-type and MFM-type stacks plotted each decade of cycles over the lifetime of the device (b).

with a repeated die over the whole 300 mm wafer surface. The device die consisted of a regular array of over 12 000 electrodes ($80 \times 60\ \mu m^2$) covering an area of $\sim 26 \times 7\ mm^2$ with an electrode material coverage of 48% after the etch process. ~6000 devices in each die were cycled in E-field with a frequency of 250 kHz, the maximum achievable frequency. Voltage was selected to give optimal performance for each stack. Each cycled die was diced from the wafer, and the x-ray beam footprint in GIXRD measurements illuminated the whole width of the die, with ~75% of the die illuminated being electrically activated. The electrode coverage in the activated area was 48%, which was sufficient to observe crystallographic changes occurring as a result of cycling. GIXRD patterns were recorded by fixing the incident angle, ω, to 0.5° and scanning the detector through 20°–65° in 2θ. Diffraction patterns were analyzed using Maud software,[14,15] in combination with crystallographic information files for various phases of HfO_2 and electrode materials. The evolution of the phase composition and orthorhombic phase crystal parameters were calculated as a function of the device lifetime. First principles simulations were performed with DFT in the CP2K package.[7] Goedecker-Teter-Hutter (GTH) pseudo-potentials with double-zeta valence polarized (DZVP) basis sets and the Perdew–Burke–Ernzerhof (PBE) functional were used. The unstrained $Pca2_1$ HfO_2 unit cell is used to build $2 \times 2 \times 2$ and $1 \times 1 \times 10$ supercells, containing 96 and 120 atoms, respectively [Fig. 2(a)]. The atomic systems were subjected to *ab initio* molecular dynamics for 100 ps at 300 K with the initial polarization oriented perpendicular to the long size of the supercell. While Rietveld refinement on such samples is extremely complex, yielding, at best, semi-quantitative trends, the results are repeatable and believable (see the supplementary material). These trends combined with density functional theory (DFT) calculations can allow the indirect measurement of these mechanisms. With other analysis techniques proving equally or more difficult in the analysis of such complex crystallography, this combination of techniques offers semi-quantitative insight into this technologically important materials system.

The phase composition, orthorhombic phase parameters, and ferroelectric response are all determined by a dynamic equilibrium of strain and strain pinning at interfaces. This equilibrium is generated by the competition between intrinsic strain (dopants) and extrinsic strain (interfaces and microstructure). The etch process for the top electrode structure with the two electrode types (TiN and Si) illustrates this nicely [Fig. 3(a)]. The electrode structure was etched into the top layers of each sample. Before top electrode etch, after crystallization anneal, TiN electrodes yield more orthorhombic phases (42%; Al-dopant) than Si electrodes (17%; Al-dopant). This difference was attributed to TiN imposing compressive in-plane strain on the hafnia and the Si electrodes imposing tensile strain. The electrode etch process removed electrode material releasing strain, inducing a reversible tetragonal to orthorhombic phase transformation within hafnia.

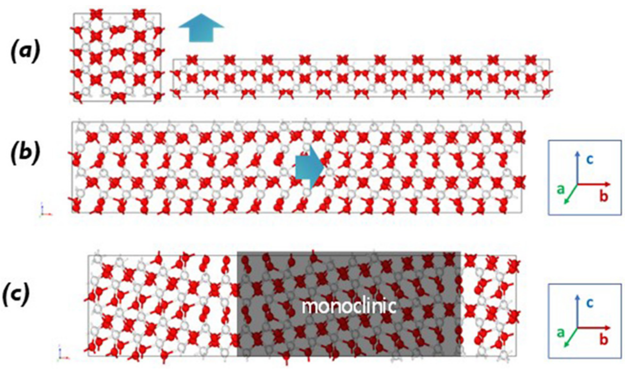

FIG. 2. Atomic models for $2 \times 2 \times 2$ (a) and $1 \times 1 \times 10$ (b) and strain accommodated (c) supercells.

Published under license by AIP Publishing

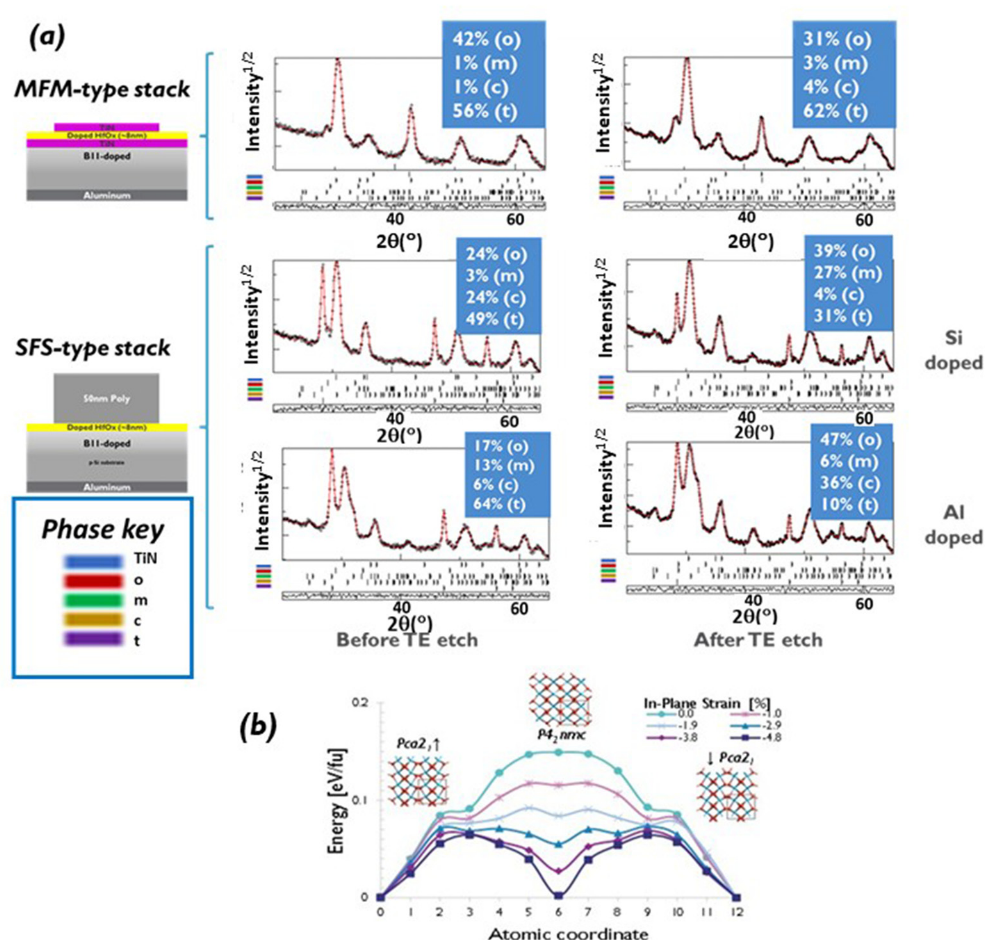

FIG. 3. Phase composition before and after top electrode etch (a) and a calculation of the modification of the potential energy landscape with strain in a tetragonal/orthorhombic phase transition (b).

When TiN was removed, the orthorhombic phase content reduced as the tetragonal phase increased. Si electrode removal yielded the converse; the orthorhombic phase content grew at the expense of tetragonal. Compressive strain during crystallization of hafnia enhances orthorhombic phase formation. Orthorhombic to tetragonal phase transformations, and vice versa, are low energy processes. This was confirmed by the DFT calculation [Fig. 3(b)], which indicates that strain can modify the potential energy landscape in this material to induce a tetragonal to orthorhombic phase transition. Furthermore, this type of transition was observed to occur with cycling in Si-doped HfO_2 layers with E-field cycling [Fig. 1(a)], a clear indication of this mechanism contributing to the wake-up process.

During E-field application, strain relaxation became important (Fig. 4). The application of the E-field induced phase transformations in all samples along with a modification of the orthorhombic unit cell parameters. In the MFM (Al:HfO_2; TiN) stack, E-field cycling yielded a measured reduction in the orthorhombic phase content along with a steady reduction in the orthorhombic unit cell volume that plateaued at $\sim$252.5 Å^3 after 10 000 cycles. This plateau corresponds to the inflection point in remnant polarization between wake-up and fatigue. Such a relaxation of the unit cell volume indicates a tendency toward a bulk-like unit cell volume where ionic shifts are more unhindered by unit cell distortion, leading to the highest polarization. Interestingly, there was a peak in the cell volume at the transition between a pinched antiferroelectric-like hysteresis and the open ferroelectric hysteresis, often the hallmark of a crystallographic transition. It should be noted that the reduction in the measured orthorhombic phase content is not consistent with the increasing remnant polarization. Instead, it suggests a crystallographic reorientation that removed the orthorhombic phase from the grazing incidence diffraction condition. Wake-up in MFM structures is typically extended with the wake-up in this sample occurring over 10 000 cycles. In SFS-type stacks, wake-up mechanisms are much quicker, which implies that strain pinning is weaker with Si electrodes, meaning that dislocations and other strain relaxing defects are easier to form. In these stacks (Al:HfO_2; Si), maximum remnant polarization was attained after 1000 cycles, with the onset of a fatigue mechanism observed immediately after. The peak in remnant polarization was accompanied by a maximum measured orthorhombic

Published under license by AIP Publishing

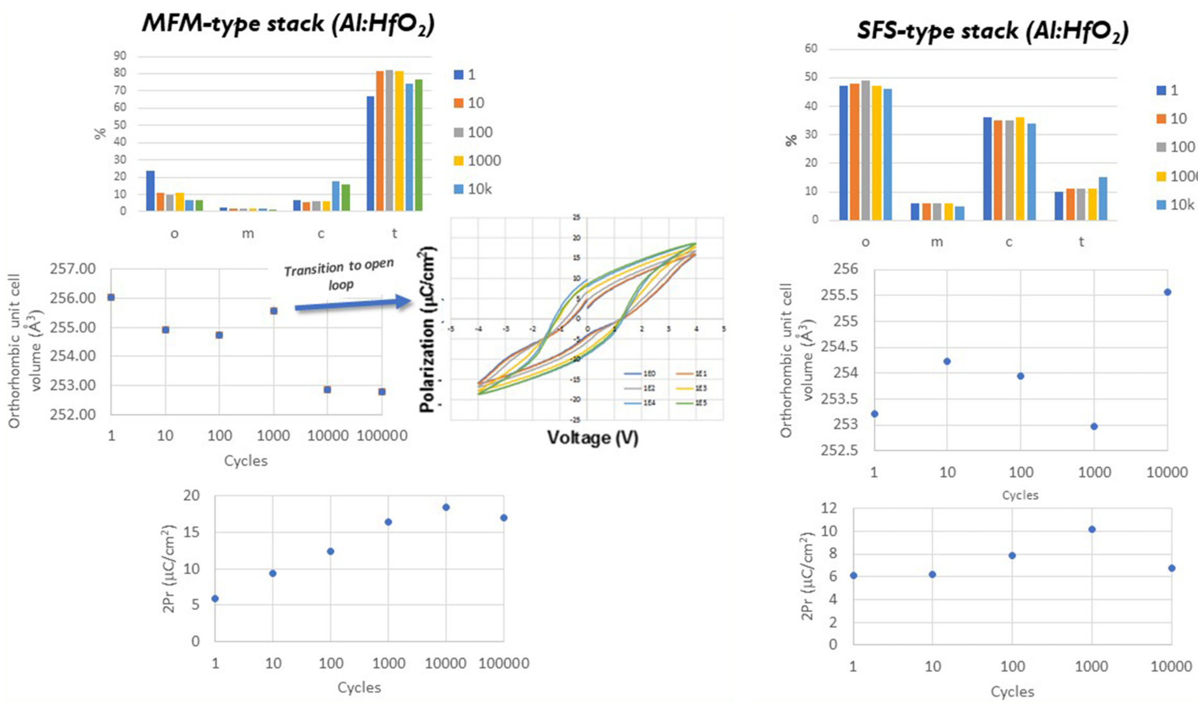

FIG. 4. Phase composition, orthorhombic unit cell volume, and remnant polarization for both MFM and SFS-type stacks as a function of E-field cycles.

phase content and a minimum in the corresponding unit cell volume of ~253 Å^3, a very similar value as in the MFM case. Both stack types relaxing to similar orthorhombic cell volumes at maximum remnant polarization further indicate that this is the bulk-like value for Al:HfO_2 and that cycling induces strain relaxation mechanisms reducing distortion in this phase's structure. Similar trends are seen in Si:HfO_2 SFS stacks, tending toward higher orthorhombic unit cell volumes.

Another mechanism that affects wake-up is the grain reorientation suggested by the data from the MFM-type cycling mentioned above. In SFS stacks (Si:HfO_2; Si), a significant drop in the orthorhombic phase was measured after the first cycle, continuing to decrease throughout the lifetime of the device (Fig. 5). This was accompanied by a significant increase in the monoclinic phase content and in the contribution of polycrystalline Si (top electrode material) to the measured phase composition of the total stack. The remnant polarization exhibited a steady increase in the initial 100 cycles, despite the measured decrease in ferroelectric material (orthorhombic phase). The GIXRD scan geometry must be considered. Due to the fixed incident angle of the x-rays, the scattering vector can never be perpendicular to the surface in these measurements. In the scans taken here, planes that are oriented $\pm 24.5°$ to the film surface were not observable. The measured increase in Si contribution, a layer unaffected by the E-field, indicated a reduction in total contribution from the hafnia layer. The reduction in the measured orthorhombic phase coinciding with an increase in remnant polarization is in line with this. The only possible explanation for increasing polarization corresponding to a measured reduction of ferroelectric material (orthorhombic phase) is an increased texture (grain reorientation) that moves orthorhombic phase planes out of the diffraction condition aligning the polarization more closely to the E-field. DFT calculations elucidated a possible mechanism; a 90° rotation of the orthorhombic structure stabilized by the monoclinic phase generation observed in GIXRD.

During the Ab Initio Molecular Dynamics (AIMD) simulation, a $2 \times 2 \times 2$ model did not depart from the initial given polarization or the crystal phase, and the symmetric supercell clamped the system constrained to the initial morphology. An unclamped $1 \times 1 \times 10$ supercell showed that the symmetry constraining factor was removed since in the long axis of the supercell, the atomic model was given an additional degree of freedom to rearrange atoms inside the supercell. As a result of this extra degree of freedom, the (higher energy) ferroelectric phase relaxed: a 90° cell rotation [Figs. 2(b) and 2(c)] transformed out-of-plane polarization into in-plane polarization. This rotation process could lead to undulations in the structure, which help the accommodation of strain, yielding monoclinic phase generation.

With this in mind, a grain reorientation mechanism for wake-up can be outlined. Starting in the first cycle, strain was applied to the orthorhombic phase domains in the hafnia layer. A reorientation of the orthorhombic phase domains occurred, preferentially affecting domains with the polarization direction oriented away from the E-field direction. With more orthorhombic domains aligned to the E-field, remnant polarization increased, reducing the orthorhombic phase contribution to the GIXRD pattern due to geometrical restraints of the measurement. The Si contribution to the phase composition, therefore, increased as the total hafnia contribution to the diffraction pattern reduced. The grain reorientation resulted in an increase in the monoclinic phase, which acted to stabilize the final strain-released structure.

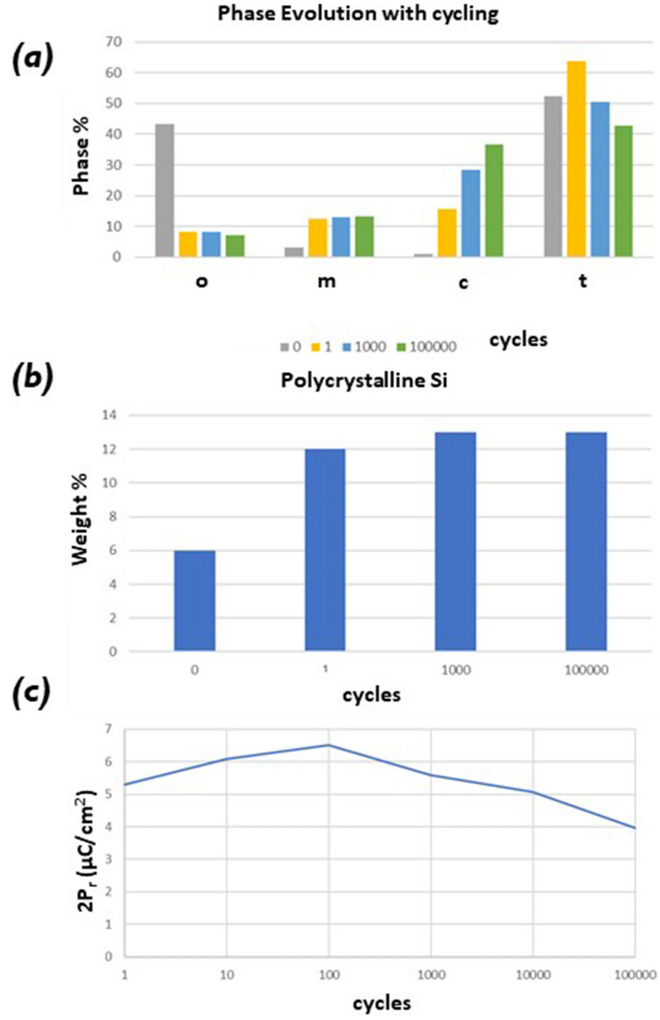

FIG. 5. Phase composition of Si:HfO_2 with E-field cycles (a), top electrode (Si) phase contribution (b), and remnant polarization (c).

The indirect measurements presented here allow the construction of a semi-quantitative, yet detailed, model of the wake-up in ferroelectric doped hafnia. The complex multiphasic nature of hafnia coupled with intrinsic and extrinsic strain effects is key. Low energy barriers for phase transformations provided wake-up under cycling with reversible tetragonal to orthorhombic conversions observed, orthorhombic to monoclinic phase transitions, and others. The orthorhombic phase relaxed toward a bulk-like unit cell volume allowing greater polarization. Finally, a model for a grain reorientation mechanism was developed. A process of 90° orthorhombic cell rotation allowed the polarization direction to further align with the E-field direction, enhancing measured remnant polarization and aiding wake-up in these structures. Although through the indirect measurement, this work demonstrates three main wake-up mechanisms for this technologically important materials system, it is hoped that these results add clarity to this field while inspiring further experiments using new techniques with greater accuracy to fully understand wake-up in ferroelectric hafnia.

See the supplementary material for a description of the GIXRD procedures explaining the fitting routine with proven repeatability and a detailed description of the E-field cycling experimental setup, assumptions, and conditions for accepted results.

DATA AVAILABILITY

The data that support the findings of this study are available from the corresponding author upon reasonable request.

REFERENCES

[1]J. Müller, U. Schröder, T. S. Böscke, I. Müller, U. Böttger, L. Wilde, J. Sundqvist, M. Lemberger, P. Kücher, T. Mikolajick, and L. Frey, "Ferroelectricity in yttrium-doped hafnium oxide," J. Appl. Phys. **110**(11), 114113 (2011).
[2]K. Florent, S. Lavizzari, M. Popovici, L. Di Piazza, U. Celano, G. Groeseneken, and J. Van Houdt, "Understanding ferroelectric Al:HfO_2 thin films with Si-based electrodes for 3D applications," J. Appl. Phys. **121**(20), 204103 (2017).
[3]E. T. Breyer, H. Mulaosmanovic, T. Mikolajick, and S. Slesazeck, "Reconfigurable NAND/NOR logic gates in 28 nm HKMG and 22 nm FD-SOI FeFET technology," in *2017 IEEE International Electron Devices Meeting (IEDM), San Francisco, CA* (IEEE, 2017), pp. 28.5.1–28.5.4.
[4]H. Mulaosmanovic, J. Ocker, S. Muller, M. Noack, J. Muller, P. Polakowski, T. Mikolajick, and S. Slesazeck, "Novel ferroelectric FET based synapse for neuromorphic systems," in *2017 Symposium on VLSI Technology, Kyoto, Japan* (IEEE, 2017), pp. T176–T177.
[5]S. Dunkel, M. Trentzsch, R. Richter, P. Moll, C. Fuchs, O. Gehring, M. Majer, S. Wittek, B. Muller, T. Melde, H. Mulaosmanovic, S. Slesazeck, S. Muller, J. Ocker, M. Noack, D.-A. Lohr, P. Polakowski, J. Muller, T. Mikolajick, J. Hontschel, B. Rice, J. Pellerin, and S. Beyer, "A FeFET based super-low-power ultra-fast embedded NVM technology for 22 nm FDSOI and beyond," in *2017 IEEE International Electron Devices Meeting (IEDM), San Francisco, CA, USA* (IEEE, 2017), pp 19.7.1–19.7.4.
[6]H. Mulaosmanovic, J. Ocker, S. Müller, U. Schroeder, J. Müller, P. Polakowski, S. Flachowsky, R. van Bentum, T. Mikolajick, and S. Slesazeck, "Switching kinetics in nanoscale hafnium oxide based ferroelectric field-effect transistors," ACS Appl. Mater. Interfaces **9**(4), 3792–3798 (2017).
[7]M. H. Park, T. Schenk, C. M. Fancher, E. D. Grimley, C. Zhou, C. Richter, J. M. LeBeau, J. L. Jones, T. Mikolajick, and U. Schroeder, "A comprehensive study on the structural evolution of HfO_2 thin films doped with various dopants," J. Mater. Chem. C **5**(19), 4677–4690 (2017).
[8]X. Sang, E. D. Grimley, T. Schenk, U. Schroeder, and J. M. LeBeau, "On the structural origins of ferroelectricity in HfO_2 thin films," Appl. Phys. Lett. **106**(16), 162905 (2015).
[9]M. H. Park, H. J. Kim, G. Lee, J. Park, Y. H. Lee, Y. J. Kim, T. Moon, K. D. Kim, S. D. Hyun, H. W. Park, H. J. Chang, J.-H. Choi, and C. S. Hwang, "A comprehensive study on the mechanism of ferroelectric phase formation in hafnia-zirconia nanolaminates and superlattices," Appl. Phys. Rev. **6**(4), 041403 (2019).
[10]S. L. Weeks, A. Pal, V. K. Narasimhan, K. A. Littau, and T. Chiang, "Engineering of ferroelectric HfO_2–ZrO_2 nanolaminates," ACS Appl. Mater. Interfaces **9**(15), 13440–13447 (2017).
[11]M. Hyuk Park, H. Joon Kim, Y. Jin Kim, W. Lee, T. Moon, and C. Seong Hwang, "Evolution of phases and ferroelectric properties of thin $Hf_{0.5}Zr_{0.5}O_2$ films according to the thickness and annealing temperature," Appl. Phys. Lett. **102**(24), 242905 (2013).
[12]T. Ali, P. Polakowski, S. Riedel, T. Büttner, T. Kämpfe, M. Rudolph, B. Pätzold, K. Seidel, D. Löhr, R. Hoffmann, M. Czernohorsky, K. Kühnel, X. Thrun, N. Hanisch, P. Steinke, J. Calvo, and J. Müller, "Silicon doped hafnium oxide (HSO) and hafnium zirconium oxide (HZO) based FeFET: A

material relation to device physics," Appl. Phys. Lett. **112**(22), 222903 (2018).
[13]U. Celano, A. Gomez, P. Piedimonte, S. Neumayer, L. Collins, M. Popovici, K. Florent, S. R. C. McMitchell, P. Favia, C. Drijbooms, H. Bender, K. Paredis, L. Di Piazza, S. Jesse, J. Van Houdt, and P. van der Heide, "Ferroelectricity in Si-doped hafnia: Probing challenges in absence of screening charges," Nanomaterials **10**(8), 1576 (2020).
[14]L. Lutterotti, S. Matthies, H.-R. Wenk, A. S. Schultz, and J. W. Richardson, "Combined texture and structure analysis of deformed limestone from time-of-flight neutron diffraction spectra," J. Appl. Phys. **81**(2), 594–600 (1997).
[15]L. Lutterotti, D. Chateigner, S. Ferrari, and J. Ricote, "Texture, residual stress and structural analysis of thin films using a combined x-ray analysis," Thin Solid Films **450**(1), 34–41 (2004).

Published under license by AIP Publishing